Breast Cancer Research

RESEARCH

Open Access

Quantifying tumor morphological complexity based on pretreatment MRI fractal analysis for predicting pathologic complete response and survival in breast cancer: a retrospective, multicenter study

Yao Huang[1,2], Ying Cao[1,2], Huifang Chen[2], Xiaosong Lan[2], Sun Tang[2], Zhitao Zhang[3], Ting Yin[4], Xiaoxia Wang[2*] and Jiuquan Zhang[2*]

Abstract

Background The tumor morphological complexity is closely associated with treatment response and prognosis in patients with breast cancer. However, conveniently quantifiable tumor morphological complexity methods are currently lacking.

Methods Women with breast cancer who underwent NAC and pretreatment MRI were retrospectively enrolled at four centers from May 2010 to April 2023. MRI-based fractal analysis was used to calculate fractal dimensions (FDs), quantifying tumor morphological complexity. Features associated with pCR were identified using multivariable logistic regression analysis, upon which a nomogram model was developed, and assessed by the area under the receiver operating characteristic curve (AUC). Cox proportional hazards analysis was used to identify independent prognostic factors for disease-free survival (DFS) and overall survival (OS) and develop nomogram models.

Results A total of 1109 patients (median age, 49 years [IQR, 43-54 years]) were included. The training, external validation cohort 1, and cohort 2 included 435, 351, and 323 patients, respectively. HR status (odds ratio [OR], 0.234 [0.135, 0.406]; $P < 0.001$), HER2 status (OR, 3.320 [1.923, 5.729]; $P < 0.001$), and Global FD (OR, 0.352 [0.261, 0.480]; $P < 0.001$) were independent predictors of pCR. The nomogram model for predicting pCR achieved AUCs of 0.80 (95% CI: 0.75, 0.86) and 0.74 (95% CI: 0.68, 0.79) in the external validation cohorts. The nomogram model, which integrated global FD and clinicopathological variables can stratify prognosis into low-risk and high-risk groups (*log-rank test*, DFS: $P = 0.04$; OS: $P < 0.001$).

Conclusions Global FD can quantify tumor morphological complexity and the model that combines global FD and clinicopathological variables showed good performance in predicting pCR to NAC and survival in patients with breast cancer.

Keywords Breast cancer, MRI, Pathological complete response, Neoadjuvant chemotherapy

*Correspondence:
Xiaoxia Wang
wangxx0531@foxmail.com
Jiuquan Zhang
zhangjq_radiol@foxmail.com
Full list of author information is available at the end of the article

© The Author(s) 2025. **Open Access** This article is licensed under a Creative Commons Attribution-NonCommercial-NoDerivatives 4.0 International License, which permits any non-commercial use, sharing, distribution and reproduction in any medium or format, as long as you give appropriate credit to the original author(s) and the source, provide a link to the Creative Commons licence, and indicate if you modified the licensed material. You do not have permission under this licence to share adapted material derived from this article or parts of it. The images or other third party material in this article are included in the article's Creative Commons licence, unless indicated otherwise in a credit line to the material. If material is not included in the article's Creative Commons licence and your intended use is not permitted by statutory regulation or exceeds the permitted use, you will need to obtain permission directly from the copyright holder. To view a copy of this licence, visit http://creativecommons.org/licenses/by-nc-nd/4.0/.

Introduction

Neoadjuvant chemotherapy (NAC) is the preferred treatment for locally advanced breast cancer, effectively reducing tumor size and raising the possibility of breast-conserving surgery [1, 2]. Patients who achieved pathological complete response (pCR) after NAC showed improved disease-free survival (DFS) and overall survival (OS) [3]. However, non-responders not only face increased economic burden but also potential drug side effects [4, 5]. Therefore, a reliable approach to predict pCR and prognosis is urgently required in patients with breast cancer for personalized treatment.

Tumor morphological complexity has been a manifestation of heterogeneity in breast cancer [6, 7]. Patients with higher tumor sphericity and smaller volumes are more likely to achieve pCR [8–10]. A greater size and more irregular morphology of the tumor are linked to increased risks of metastasis and recurrence [11, 12]. Consequently, there is a close correlation between tumor morphological features and treatment response and prognosis [13, 14]. Despite the variety of features used to describe tumor morphology, many techniques essentially assess the same tumor characteristics, such as tumor size indicated by diameter and volume. However, models based on these traditional morphological features (e.g., sphericity and longest diameter) often show limited performance in predicting pCR to NAC, with area under the receiver operating characteristic curve (AUC) values ranging from 0.61 to 0.79 [9, 10]. This limitation may be due to the inability of traditional morphological features to fully capture the complexity and heterogeneity of tumor morphology. Additionally, these models lack external validation in large, multicenter studies, which limits their reliability in clinical decision-making. Therefore, it is necessary to develop a quantitative parameter to more accurately quantify tumor morphological complexity, which could be valuable in predicting pCR and survival outcomes.

Fractal analysis has demonstrated utility in quantifying tumor morphological complexity by measuring self-similarity across different spatial scales [15]. Higher fractal dimension (FD) values suggest greater complexity, which may be indicative of poorer treatment outcomes and prognosis [16, 17]. Previous studies have quantitatively measured FD to distinguish between benign and malignant lesions in ultrasound, mammography, and MRI, with higher FD values more indicative of malignancy [18–21]. However, these studies primarily focused on 2D fractal analysis, which may not fully capture the morphological complexity of tumor. Dynamic contrast-enhanced (DCE-MRI) is recognized as one of the most sensitive imaging modalities for assessing the therapeutic response to NAC in breast cancer [22]. A preliminary study explored the potential of using fractal analysis of volumetric DCE-MRI pharmacokinetic parametric maps to predict pCR to NAC [23]. However, this study was limited by its single-center design and small sample size, and the prognostic value of fractal analysis remains unclear, requiring further validation. Additionally, current research lacks a clear delineation of the relationship between MRI-based morphological features of breast cancer and FD values, as well as their comparative efficacy in predicting pCR to NAC.

Thus, this study aimed to quantify tumor morphological complexity using multi-dimensional fractal analysis based on pretreatment MRI and to analyze the relationships between FDs and clinicopathologic variables, as well as between FDs and morphological features. Additionally, the study evaluated the predictive value of a model that combines FDs with clinicopathologic variables in predicting pCR to NAC and survival prognosis in patients with breast cancer.

Materials and methods

Study cohort

This multicenter retrospective study received approval from the institutional review boards of each participating center, and the requirement for patient written informed consent was waived. The study was conducted following the Transparent Reporting of a Multivariable Prediction Model for Individual Prognosis or Diagnosis (TRIPOD) guidelines [24]. A checklist is provided in Supplementary Table S1.

From May 2010 to April 2023, this study included female patients from three academic medical centers and one public dataset (I-SPY2 trial) [9]. Centers A and B served as the training cohort, while Center C and the I-SPY2 trial served as the two external validation cohorts. The inclusion criteria were: (*a*) biopsy-confirmed invasive breast cancer without distant metastasis, (*b*) MRI conducted before NAC, and (*c*) post-NAC pathological confirmation of pCR. The exclusion criteria involved: (*a*) inadequate MRI quality, the overall image quality was assessed by a radiologist (X.X.W., with 10 years of experience in breast MRI) using a 5-point Likert scale (1 = poor, 2 = subpar, 3 = moderate, 4 = good, 5 = excellent), with scores of 2 or below considered inadequate [25, 26]. (*b*) Lack of histopathologic data, (*c*) previous history of breast cancer, (*d*) external institution surgery or unassessed pCR, (*e*) incomplete clinical data (excluding uncollected characteristics), and (*f*) lack of follow-up records for survival prognosis analysis in center A (Fig. 1A).

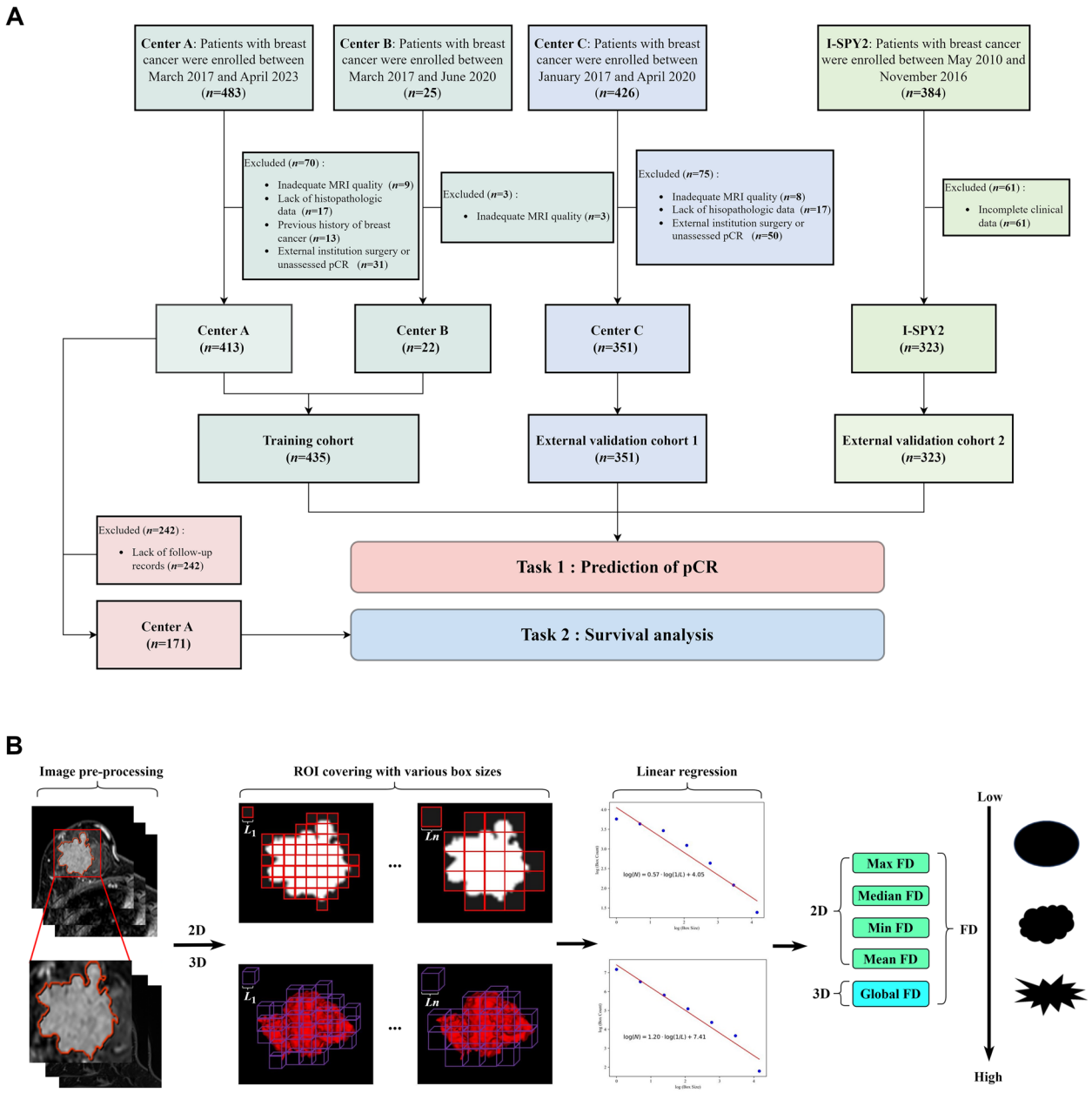

Fig. 1 Patient inclusion and exclusion process for four center (**A**) and FD calculation flowchart (**B**). The training cohort was used to develop models to predict pCR to NAC, which was then validated across the two external cohorts. Patients from center A were also included for survival analysis. Four FDs (max FD, median FD, min FD, and mean FD) were calculated from 2D slices, while one 3D FD (global FD) was calculated from the entire tumor volume. Data from the I-SPY2 trial are publicly available on The Cancer Imaging Archive. NAC = neoadjuvant chemotherapy, FD = fractal dimension, pCR = pathologic complete response

NAC regimens and histopathology analysis

All patients received an anthracyclines and/or taxanes-based NAC regimen. For human epidermal growth factor receptor2 (HER2) positive patients, treatment included trastuzumab alone or in combination with pertuzumab.

In this study, pre-NAC core needle biopsies were conducted, and immunohistochemistry determined estrogen receptor (ER), progesterone receptor (PR) status, HER2 status, and Ki-67 index status for patients from centers A, B, and C. Tumors with ≥1% nuclear staining were defined as ER (+)/PR (+), while those with < 1% as ER (-)/PR (-) [27, 28]. HR positivity is defined as ER (+) and/or PR (+). HER2 status was categorized as negative for 0 or 1+ immunohistochemistry scores, and positive for

3+ scores. For 2+ scores, fluorescence in situ hybridization (FISH) determined HER2 status; amplification signified HER2 (+), and lack thereof indicated HER2 (-) [29, 30]. Additionally, a Ki-67 index threshold of 20% was set, where ≥ 20% denoted high expression and < 20% indicated low expression [31].

The pCR was defined based on surgical pathology as the absence of residual invasive cancer, possibly with residual ductal carcinoma in situ, and no lymph node invasion in the axillary lymph nodes (ypT0/is ypN0).

MRI procedure and image processing

All MRI examinations were performed with 1.5 T or 3.0 T scanners. Detailed protocols are provided in Supplementary Table S2.

To minimize variability in imaging protocols, B-spline interpolation was used to resample images to 1×1×1 mm^3, and z-score normalization was used for image intensity standardization. The peak enhancement phase of dynamic contrast-enhanced MRI, selected based on the time-signal intensity curve, was used to delineate the regions of interest (ROI) for subsequent fractal analysis [32]. Initial semi-automatic tumor region segmentation was performed using the Dr. Wise platform (https://keyan.deepwise.com). Two radiologists (S.T., and L.L., with 6 and 10 years of experience in breast MRI, respectively) then manually corrected the segmentation. If there were multiple lesions, only the largest one was considered [33].

Image analysis

FDs were calculated using the box-counting method in MATLAB (version, R2020a) [34], with the input being delineated ROI images, resulting in both 2D FDs and 3D FD. Initially, post-segmentation images underwent binarization. Subsequently, boxes of incremental sizes covered tumor region on each slice or the entire tumor volume, recording the minimum needed for full coverage, with sizes increasing up to 45% of image dimensions [16, 35]. Finally, logarithmic transformation was applied to box sizes and corresponding quantities for linear regression via the least-squares method, as illustrated: $\log N_L = k \cdot \log L + b$, where N_L is the minimum count of boxes, each with side length L, needed to cover the ROI areas, and FD is the negative of k. It is noteworthy that the calculated FDs may vary depending on the spatial sparsity and morphological complexity of tumor structures. The codes for fractal dimension analysis are available in a GitHub repository (https://github.com/YaoHuang1123/FD).

For each patient, four 2D FDs (max FD, median FD, min FD, and mean FD) and one 3D FD (global FD) were calculated (Fig. 1B). Meanwhile, 14 morphological features describing tumor size and geometric shape were extracted [36]. Detailed descriptions of the FD calculations and morphological feature extractions can be found in the Supplementary materials.

Development of models for predicting pCR to NAC

To predict pCR to NAC, seven logistic regression models were developed. Five models were developed using individual FD parameters to compare the performance of different FD quantitative metrics in predicting pCR to NAC. A morphological model based on morphological features was constructed to evaluate its predictive performance against FDs. To further improve model performance, nomogram model-1 was developed by integrating FDs with clinicopathological variables, and nomogram model-2 was created by integrating morphological features with clinicopathological variables for comparison with nomogram model-1.

Follow-up data collection

For surveillance of recurrence and distant metastasis, patients underwent post-surgery follow-ups every six months with chest radiography and/or chest CT scans, along with annual bone scans and abdominal CT scans or ultrasounds. Follow-up was conducted in center A by two radiologists (S.T., and L.L., each with 6 and 10 years of experience), who recorded DFS and OS from the surgery date (the time origin) to the first recurrence or death, respectively. Patients without recurrence or death were censored at their last follow-up date.

Statistical analysis

Statistical analysis was conducted using R (version 4.3.1) and Python (version 3.9.5). To assess the reproducibility of fractal analysis, images from 30 patients (15 patients with pCR and 15 patients with non-pCR) randomly selected were segmented twice by a radiologist at one-month intervals and once by another radiologist. Bland-Altman statistics was used to evaluate intra-observer consistency, and a mixed-effects model with random effects on intercept and slope was used for variance-component analysis to assess the reproducibility of fractal analysis [37]. The intraclass correlation coefficient (ICC) was used to assess interobserver consistency, with an ICC > 0.75 indicating good consistency.

The χ^2 test was used to compare differences in categorical variables between the pCR and non-pCR groups when cell frequencies were greater than or equal to 5, while *Fisher* exact test was applied when any cell frequency was less than 5. The *Kolmogorov-Smirnov* test was used to assess the normal distribution of continuous variables, and the *Levene* test was applied to assess

Table 1 The characteristics of patients in three cohorts

Characteristics	Training cohort (*n* = 435)		*P* Value	External validation cohort 1 (*n* = 351)		*P* Value	External validation cohort 2 (*n* = 323)		*P* Value
	pCR (*n* = 114)	Non-pCR (*n* = 321)		pCR (*n* = 83)	Non-pCR (*n* = 268)		pCR (*n* = 97)	Non-pCR (*n* = 226)	
Age (years)*	51 (45–55)	50 (46–55)	.58‡	49 ± 8	47 ± 9	.11†	49 (41–56)	47 (40–56)	.72‡
Age group									
≤ 45	40 (35)	104 (32)		21 (25)	112 (42)		40 (41)	45 (41)	
> 45	74 (65)	217 (68)		62 (75)	156 (58)		57 (59)	134 (59)	
Menopausal status			.94⁑			.34⁑			.27⁑
Premenopausal	70 (61)	194 (60)		50 (60)	179 (67)		51 (53)	140 (62)	
Postmenopausal	44 (39)	127 (40)		33 (40)	89 (33)		39 (40)	75 (33)	
Perimenopausal	0 (0)	0 (0)		0 (0)	0 (0)		7 (7)	11 (5)	
HR status			<.001⁑			<.001⁑			<.001⁑
Negative	76 (67)	91 (28)		49 (59)	78 (29)		59 (61)	78 (35)	
Positive	38 (33)	230 (72)		34 (41)	190 (71)		38 (39)	148 (65)	
HER2 status			<.001⁑			<.001⁑			.02⁑
Negative	45 (39)	224 (70)		45 (54)	206 (77)		66 (68)	183 (81)	
Positive	69 (61)	97 (30)		38 (46)	62 (23)		31 (32)	43 (19)	
Ki-67 status			.01⁑			<.001⁑			
Low (< 20%)	9 (8)	63 (20)		8 (10)	83 (31)		0 (0)	0 (0)	
High (≥ 20%)	105 (92)	258 (80)		75 (90)	185 (69)		0 (0)	0 (0)	
Not available	0 (0)	0 (0)		0 (0)	0 (0)		97 (100)	226 (100)	
Clinical T stage			.11⁑						
cT1	11 (9)	25 (8)		0 (0)	0 (0)		0 (0)	0 (0)	
cT2	61 (54)	136 (42)		0 (0)	0 (0)		0 (0)	0 (0)	
cT3	17 (15)	57 (18)		0 (0)	0 (0)		0 (0)	0 (0)	
cT4	25 (22)	103 (32)		0 (0)	0 (0)		0 (0)	0 (0)	
Not available	0 (0)	0 (0)		83 (100)	268 (100)		97 (100)	226 (100)	
Clinical N stage			0.37⁑						
cN0	11 (10)	39 (12)		0 (0)	0 (0)		0 (0)	0 (0)	
cN1	45 (39)	103 (32)		0 (0)	0 (0)		0 (0)	0 (0)	
cN2	43 (38)	120 (38)		0 (0)	0 (0)		0 (0)	0 (0)	
cN3	15 (13)	59 (18)		0 (0)	0 (0)		0 (0)	0 (0)	
Not available	0 (0)	0 (0)		83 (100)	268 (100)		97 (100)	226 (100)	
Molecular subtypes			<.001⁑			<.001⁑			<.001⁑
HR+/HER2-	11 (10)	165 (52)		19 (23)	153 (57)		22 (23)	115 (51)	
HR+/HER2+	27 (23)	65 (20)		15 (18)	37 (14)		16 (17)	33 (15)	
HR-/HER2-	34 (30)	59 (18)		26 (31)	53 (20)		44 (45)	68 (30)	
HR-/HER2+	42 (37)	32 (10)		23 (28)	25 (9)		15 (15)	10 (4)	
FD									
Max FD	1.37 ± 0.21	1.46 ± 0.15	<.001‡	1.34 ± 0.18	1.40 ± 0.17	.01‡	1.51 ± 0.15	1.55 ± 0.14	.01‡
Median FD	1.26 ± 0.20	1.34 ± 0.15	<.001‡	1.20 ± 0.19	1.26 ± 0.18	.01‡	1.42 ± 0.14	1.46 ± 0.14	.06‡
Min FD	0.97 ± 0.18	1.02 ± 0.18	.01†	1.01 ± 0.20	0.99 ± 0.21	.796†	1.26 ± 0.17	1.28 ± 0.18	.12‡
Mean FD	1.23 ± 0.19	1.31 ± 0.14	<.001‡	1.19 ± 0.18	1.24 ± 0.17	.046‡	1.41 ± 0.14	1.44 ± 0.14	.06‡
Global FD	1.75 ± 0.31	2.00 ± 0.21	<.001‡	1.77 ± 0.24	1.95 ± 0.22	<.001‡	1.89 ± 0.20	2.02 ± 0.20	<.001†

Unless otherwise indicated, numbers represent the count of patients, with percentages in parentheses

P values indicate the comparison of characteristics between the pCR and non-pCR groups across different cohorts

FD fractal dimension, *HER2* human epidermal growth factor receptor2, *HR* hormone receptor, *pCR* pathologic complete response

* Data are medians, with IQRs in parentheses

‡ Mann–Whitney U test

† *t*-test

⁑ χ^2 test or fisher exact test

homogeneity. If the data met both normality and homogeneity of variance, group differences were compared using the *t-test*; otherwise, the *Mann-Whitney U* test was applied. Univariable and multivariable logistic regression analyses were performed to assess the association between features and pCR, and molecular subtypes were excluded from the multivariable logistic regression model because of their collinearity with both HR status and HER2 status. Independent predictors of pCR were used to create a nomogram model. Model performance was assessed by AUC, and accuracy, sensitivity specificity, positive predictive value, and negative predictive value were also calculated. AUCs of different models were compared using the Delong test. The *Hosmer-Lemeshow* test assessed the calibration of models, and decision curves were used to evaluate the benefit of models. The correlation coefficients were calculated using Spearman correlation analysis.

The survival analysis used Cox proportional hazards analysis to identify factors associated with survival outcomes (DFS and OS) and develop nomogram models. Patients were divided into high and low-score groups

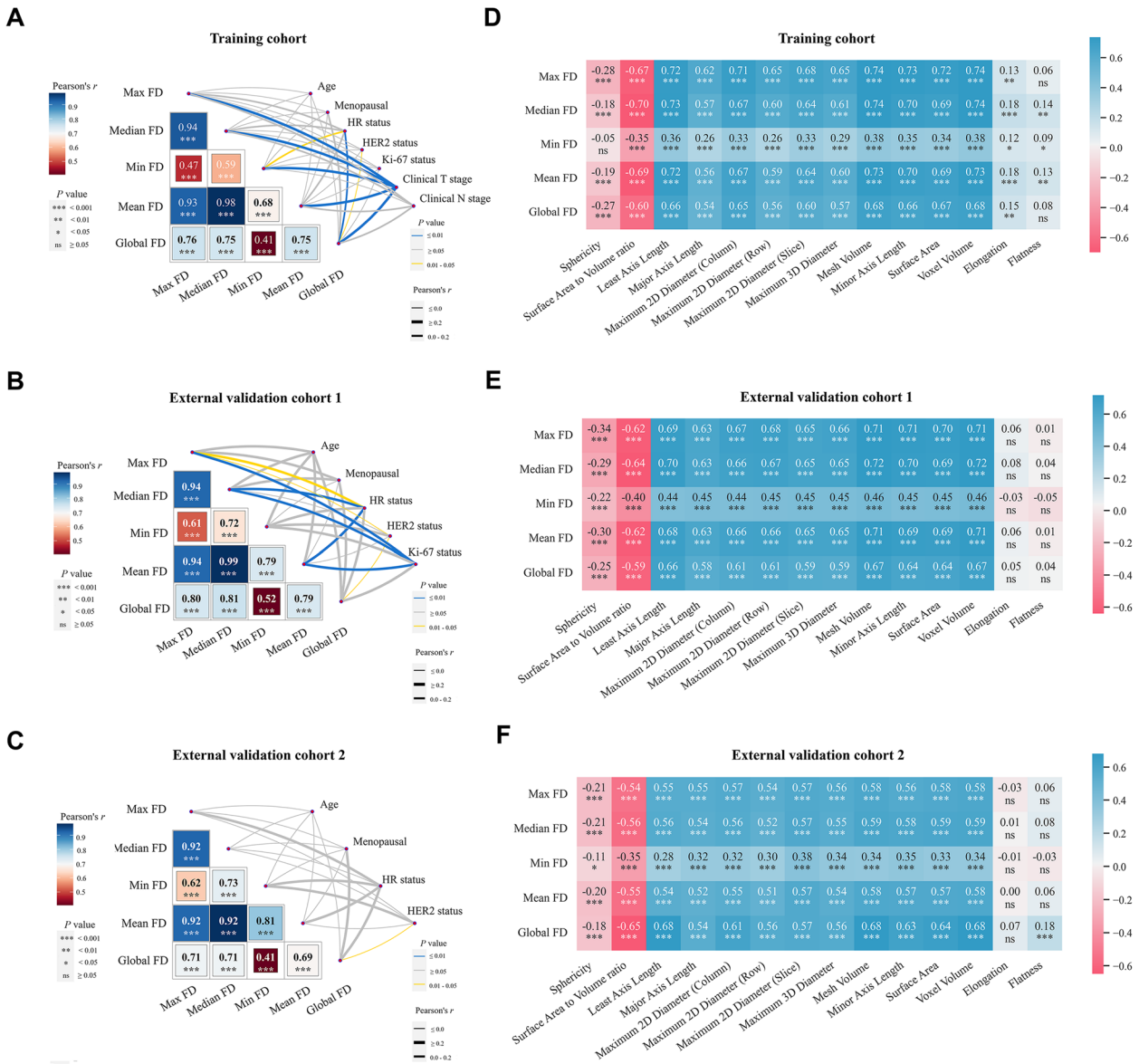

Fig. 2 The Spearman correlation coefficient network diagrams (**A**-**C**) between FDs and clinicopathologic variables, and the Spearman correlation coefficient heat maps (**D**-**F**) between FDs and morphological features in the training cohort, external validation cohort 1, and external validation cohort 2, respectively. The global FD showed a negative correlation with HER2 status, sphericity, and surface area to volume ratio, while it was positively correlated with diameter and volume. FD = fractal dimension, HER2 = human epidermal growth factor receptor 2, HR = hormone receptor

based on the median score of the nomogram model. Differences in DFS and OS between these groups were compared using Kaplan-Meier curves and the *Log-rank* test. Two-tailed $P < 0.05$ was deemed statistically significant.

Results

Baseline characteristics

In this study, 1318 patients were initially acquired from three academic medical centers and one public dataset. Patients were excluded for inadequate MRI quality ($n = 20$), lack of histopathologic data ($n = 34$), previous history of breast cancer ($n = 13$), external institution surgery or unassessed pCR ($n = 81$), and incomplete clinical data ($n = 61$), resulting in 1109 patients being included in the study (Fig. 1A). For predicting pCR, the training cohort comprised 435 patients (center A [$n = 413$], center B [$n = 22$]; median age, 51 years [IQR, 46–55 years]). Two external validation cohorts consisted of 351 patients from center C (median age, 48 years [IQR, 43–52 years]) and 323 patients from I-SPY2 (median age, 48 years [IQR, 40–56 years]).

In all cohorts, significant differences were observed in HR status, HER2 status, max FD, and global FD between pCR and non-pCR groups (all $P < 0.05$) (Table 1).

Reproducibility of fractal analysis

The FDs for both 3D and 2D fractal analysis showed good consistency, the Bland-Altman repeatability coefficients ranging from 0.11 to 0.19 (Supplementary Table S3 and Fig. S1). Variance-components analysis indicated that

Table 2 Univariable and multivariable logistic regression analysis of characteristics associated with pCR in the training cohort

Characteristics	Univariable Odds Ratio (95% CI)	*P* Value	Multivariable Odds Ratio (95% CI)	*P* Value
Age	0.896 (0.725, 1.108)	0.312		
Menopausal status				
Premenopausal	Reference			
Postmenopausal	0.960 (0.619, 1.489)	0.856		
HR status				
Negative	Reference			
Positive	0.197 (0.125, 0.313)	< 0.001	0.234 (0.135, 0.406)	< 0.001
HER2 status				
Negative	Reference			
Positive	3.541 (2.270, 5.524)	<0.001	3.320 (1.923, 5.729)	< 0.001
Ki-67 status				
Low	Reference			
High	2.849 (1.367, 5.937)	0.005	2.023 (0.785, 5.214)	0.145
Clinical T stage				
cT1	Reference			
cT2	1.222 (0.734, 2.036)	0.441	0.903 (0.331, 2.468)	0.843
cT3	0.812 (0.450, 1.463)	0.488	0.718 (0.220, 2.335)	0.581
cT4	0.595 (0.360, 0.982)	0.042	0.497 (0.161, 1.527)	0.222
Clinical N stage				
cN0	Reference			
cN1	1.380 (0.887, 2.149)	0.154		
cN2	1.014 (0.653, 1.577)	0.949		
cN3	0.673 (0.365, 1.241)	0.204		
Molecular subtypes				
HR+/HER2-	Reference			
HR+/HER2+	1.222 (0.734, 2.036)	0.441		
HR-/HER2-	1.887 (1.155, 3.083)	0.011		
HR-/HER2+	5.268 (3.109, 8.927)	< 0.001		
FD				
Global FD	0.340 (0.256, 0.451)	< 0.001	0.352 (0.261, 0.480)	< 0.001

Data in parentheses are 95% CI. Molecular subtypes were excluded from the multivariable logistic regression model because of their collinearity with both HR status and HER2 status

CI confidence interval, *FD* fractal dimension, *HER2*= human epidermal growth factor receptor2, *HR* hormone receptor, pCR pathologic complete response

the variance between patients (variance:0.0172–0.0195) exceeded the variance between readings (variance: 0.0001–0.0009) for both 3D and 2D fractal analyses. The coefficient of variation (COV) for 2D FDs (COV: 3.21–6.78) between readings was found to be higher than that for 3D (COV: 2.65), whereas the coefficient of variation for 2D FDs (COV: 377.94–467.28) between patients was lower compared to 3D (486.94). Furthermore, five FDs showed good inter-observer consistency (ICC: 0.87–0.93) (Supplementary Table S4).

Correlation analysis

Spearman correlation analysis indicated that global FD strongly positively correlated with max, median, and mean FD (correlation coefficient [*r*]: 0.69 to 0.81, $P < 0.05$), and negatively with HER2 status (*r*: −0.12 to −0.01, $P \leq 0.04$). Global FD showed negative correlations with sphericity and surface area to volume ratio (*r*: −0.65 to −0.18, $P \leq 0.04$), and positively with diameter and volume (*r*: 0.54 to 0.68, $P \leq 0.04$) (Fig. 2, Supplementary Table S5 and S6).

Variables associated with pCR

Univariable logistic regression analysis showed that HR status, HER2 status, Ki-67 status, Clinical T stage, and global FD were associated with pCR. After adjustment of the multivariable model for variables with $P < 0.05$ in the univariable analysis, HR status (odds ratio [OR], 0.234 [95% CI: 0.135, 0.406]; $P < 0.001$), HER2 status (OR, 3.320 [95% CI: 1.923, 5.729]; $P < 0.001$), and global FD (OR, 0.352 [95% CI: 0.261, 0.480]; $P < 0.001$) were independent predictors for pCR (Table 2). These independent predictors were then used to develop the nomogram model-1. Following the same process, clinicopathological variables

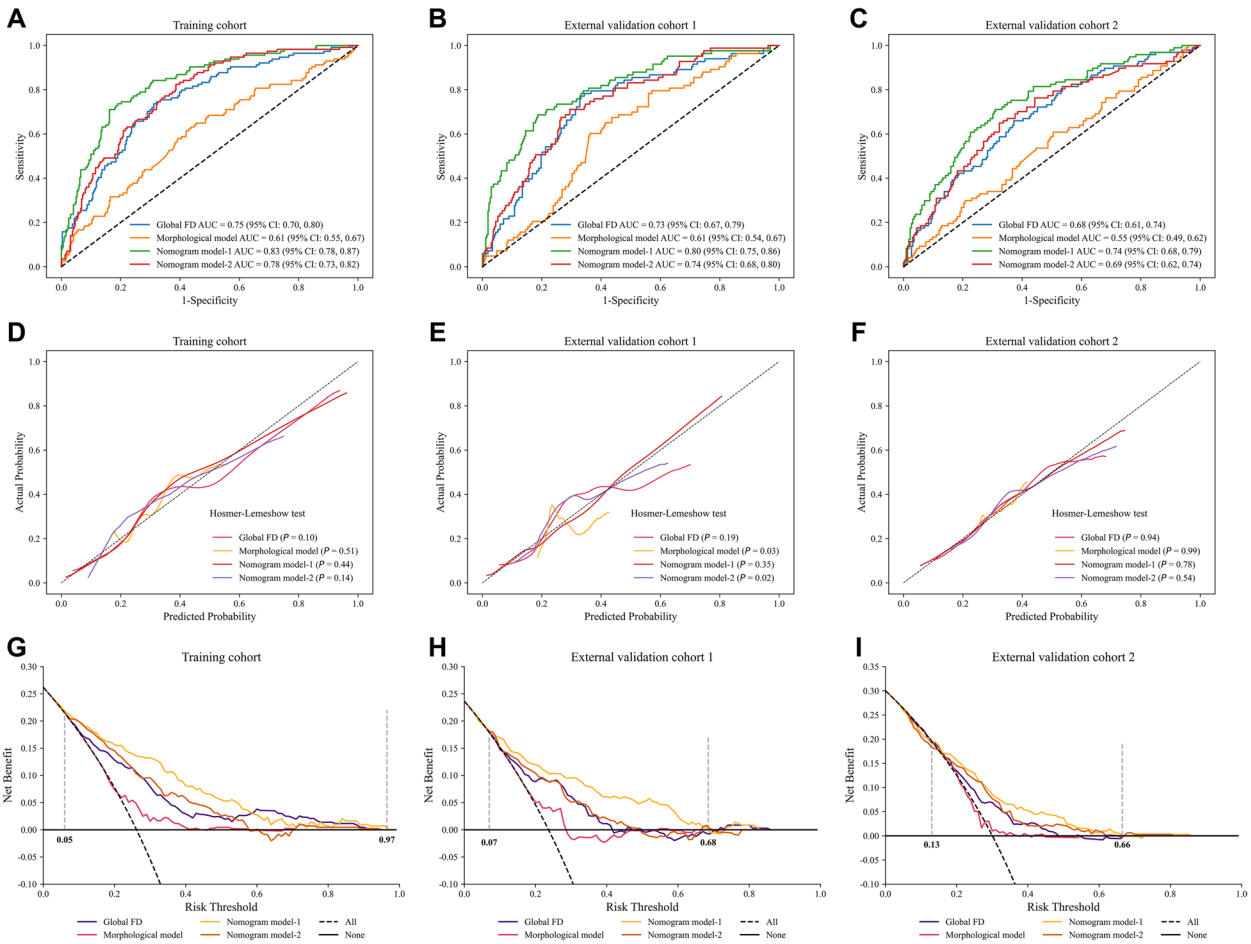

Fig. 3 The receiver operating characteristic curves (**A**-**C**), calibration curve (**D**-**F**) and decision curves (**G**-**I**) of different models in the training cohort, external validation cohort 1, and external validation cohort 2, respectively. The morphological model incorporates sphericity, major axis length and maximum 2D diameter (row). The nomogram model-1 integrates hormone receptor, human epidermal growth factor receptor-2, and global FD. The nomogram model-2 integrates hormone receptor, human epidermal growth factor receptor-2, sphericity, major axis length and maximum 2D diameter (row). The nomogram model-1 showed the best performance in predicting pCR to NAC. AUC = area under the receiver operating characteristic curve, CI = confidence interval, FD = fractal dimension

Table 3 Performances of different models for predicting pCR to NAC in three cohorts

Cohorts	Models	AUC (95% CI)	ACC (%)	SEN (%)	SPE (%)	PPV (%)	NPV (%)
TC	Global FD	0.75 (0.70, 0.80)	70.1	73.7	68.8	45.7	88.0
	Morphological model	0.61 (0.55, 0.67)	58.2	63.2	56.4	34.0	81.2
	Nomogram model-1	0.83 (0.78, 0.87)	80.5	71.1	83.8	60.9	89.1
	Nomogram model-2	0.78 (0.73, 0.82)	66.9	82.5	61.4	43.1	90.8
EVC-1	Global FD	0.73 (0.67, 0.79)	67.2	79.5	63.4	40.2	90.9
	Morphological model	0.61 (0.54, 0.67)	63.0	60.2	63.8	34.0	83.8
	Nomogram model-1	0.80 (0.75, 0.86)	78.3	67.5	81.7	53.3	89.0
	Nomogram model-2	0.74 (0.68, 0.80)	70.7	71.1	70.5	42.8	88.7
EVC-2	Global FD	0.68 (0.61, 0.74)	65.6	53.6	70.8	44.1	78.0
	Morphological model	0.55 (0.49, 0.62)	52.9	60.8	49.6	34.1	74.7
	Nomogram model-1	0.74 (0.68, 0.79)	72.4	38.1	87.2	56.1	76.7
	Nomogram model-2	0.69 (0.62, 0.74)	66.9	64.9	67.7	46.3	81.8

Nomogram model-1: combining hormone receptor, human epidermal growth factor receptor-2 and global FD

Nomogram model-2: combining hormone receptor, human epidermal growth factor receptor-2, sphericity, major axis length and maximum 2D diameter (row)

AUC area under the receiver operating characteristic curve, *ACC* accuracy, *CI* confidence interval, *SEN* sensitivity, *SPE* specificity, *PPV* positive predictive value, *NPV* negative predictive value, *TC* training cohort, *EVC-1* external validation cohort 1, *EVC-2* external validation cohort 2

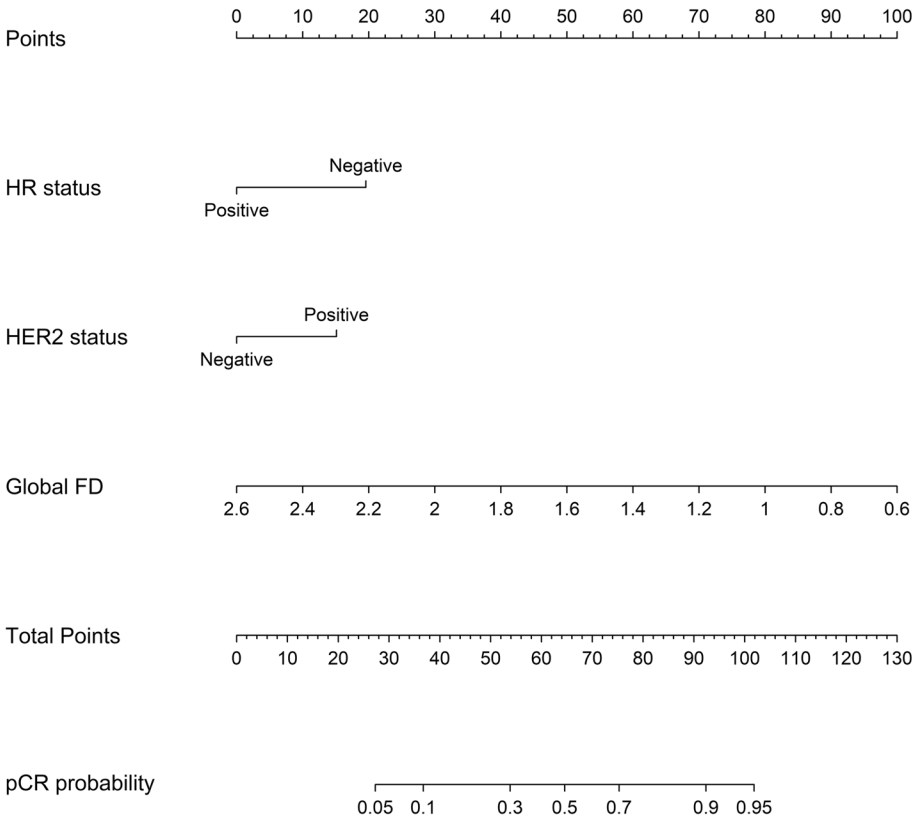

Fig. 4 A nomogram model incorporating hormone receptor, human epidermal growth factor receptor-2 and global FD for predicting pCR to NAC. The nomogram model indicated that patients with HR-negative, HER2-positive status and lower global FD values are more likely to achieve pCR after NAC. FD = fractal dimension, HER2 = human epidermal growth factor receptor2, HR = hormone receptor, pCR = pathologic complete response

(HR and HER2 status) and morphological features (sphericity, major axis length, and maximum 2D diameter [row]) were identified to develop the nomogram model-2 (Supplementary Table S7).

Performance of models for prediction of pCR

For predicting pCR to NAC, the AUCs ranging from 0.52 to 0.73 were observed for five FD univariable models across two external validation cohorts (Supplementary Fig. S2). Global FD achieved AUCs of 0.73 (95% CI: 0.67, 0.79) and 0.68 (95% CI: 0.61, 0.74), significantly outperforming morphological models with AUCs of 0.61 (95% CI: 0.54, 0.64) and 0.55 (95% CI: 0.49, 0.62) in the two external validation cohorts (Delong test, all $P < 0.001$), respectively (Fig. 3A-C, Table 3, Supplementary Table S8).

The nomogram model-1 achieved AUCs of 0.80 (95% CI: 0.75, 0.86) and 0.74 (95% CI: 0.68, 0.79) (Figs. 3A-C and 4), significantly outperforming nomogram model-2 with AUCs of 0.74 (95% CI: 0.68, 0.80) and 0.69 (95% CI: 0.62, 0.74) in two external validation cohorts, respectively (Delong test, $P < 0.001$) (Supplementary Table S8).

The calibration between predicted and observed probabilities was good for nomogram model-1 (*Hosmer-Lemeshow* test, *P*: 0.35–0.78) (Fig. 3D-F). Decision curve analysis showed that nomogram model-1 offered greater clinical benefit across most threshold ranges and demonstrated net benefits in two external validation cohorts at thresholds of 0.07 to 0.68 and 0.13 to 0.66 (Fig. 3G-I).

Model performance for prediction of pCR in patient subgroups

Four subgroup analyses were conducted based on molecular subtypes, age, menopausal status, and Ki-67 status. In two external validation cohorts, the global FD for prediction of pCR to NAC achieved AUCs ranging from 0.65–0.83 for patients with four molecular subtypes (HR+/HER2-, HR+/HER2+, HR-/HER2-, and HR-/HER+) (Supplementary Fig. S3).

The nomogram model-1 achieved AUCs ranging from 0.72–0.83 for patients with age ≤ 45 years or age > 45 years, and 0.74–0.82 for premenopausal or postmenopausal patients in the two external validation cohorts. For patients with high and low Ki-67 expression, the nomogram model-1 achieved AUCs of 0.77 (95% CI: 0.69–0.85) and 0.80 (95% CI: 0.79–0.82) in external validation cohort 1 (Supplementary Fig. S4).

Survival analysis

For survival analysis, 171 patients from center A (median age, 50 years [IQR, 45–55 years]) were enrolled. During the follow-up (DFS: median, 29 months [IQR, 15–44 months]; OS: median, 37 months [IQR, 18.05–48.85 months]), 52 patients had recurrence and 14 patients died (Table 4).

Table 4 The characteristics of patients for survival analysis

Characteristics	Total ($n = 171$)
Age (years)[a]	50 (45–55)
Age group	
≤ 45	48 (28)
> 45	123 (72)
Menopausal status	
Premenopausal	102 (60)
Postmenopausal	69 (40)
HR status	
Negative	74 (43)
Positive	97 (57)
HER2 status	
Negative	108 (63)
Positive	63 (37)
Ki-67 status	
Low (< 20%)	22 (13)
High (≥ 20%)	149 (87)
Clinical T stage	
cT1	17 (10)
cT2	90 (53)
cT3	36 (21)
cT4	28 (16)
Clinical N stage	
cN0	20 (12)
cN1	55 (32)
cN2	67 (39)
cN3	29 (17)
Treatment response	
Non-pCR	133 (78)
pCR	38 (22)
Global_FD	1.94 ± 0.25
DFS	
Follow-up time (DFS)[a]	20.1 (5.85–36.0)
Recurrence	52 (30)
No recurrence	119 (70)
OS	
Follow-up time (OS)[a]	36.9 (18.05–48.85)
Death	14 (8)
Survival	157 (92)

Unless otherwise indicated, numbers represent the count of patients, with percentages in parentheses

DFS Disease-free survival, *FD* fractal dimension, *HER2* human epidermal growth factor receptor2, *HR* hormone receptor, *OS* overall survival

[a] Data are medians, with IQRs in parentheses

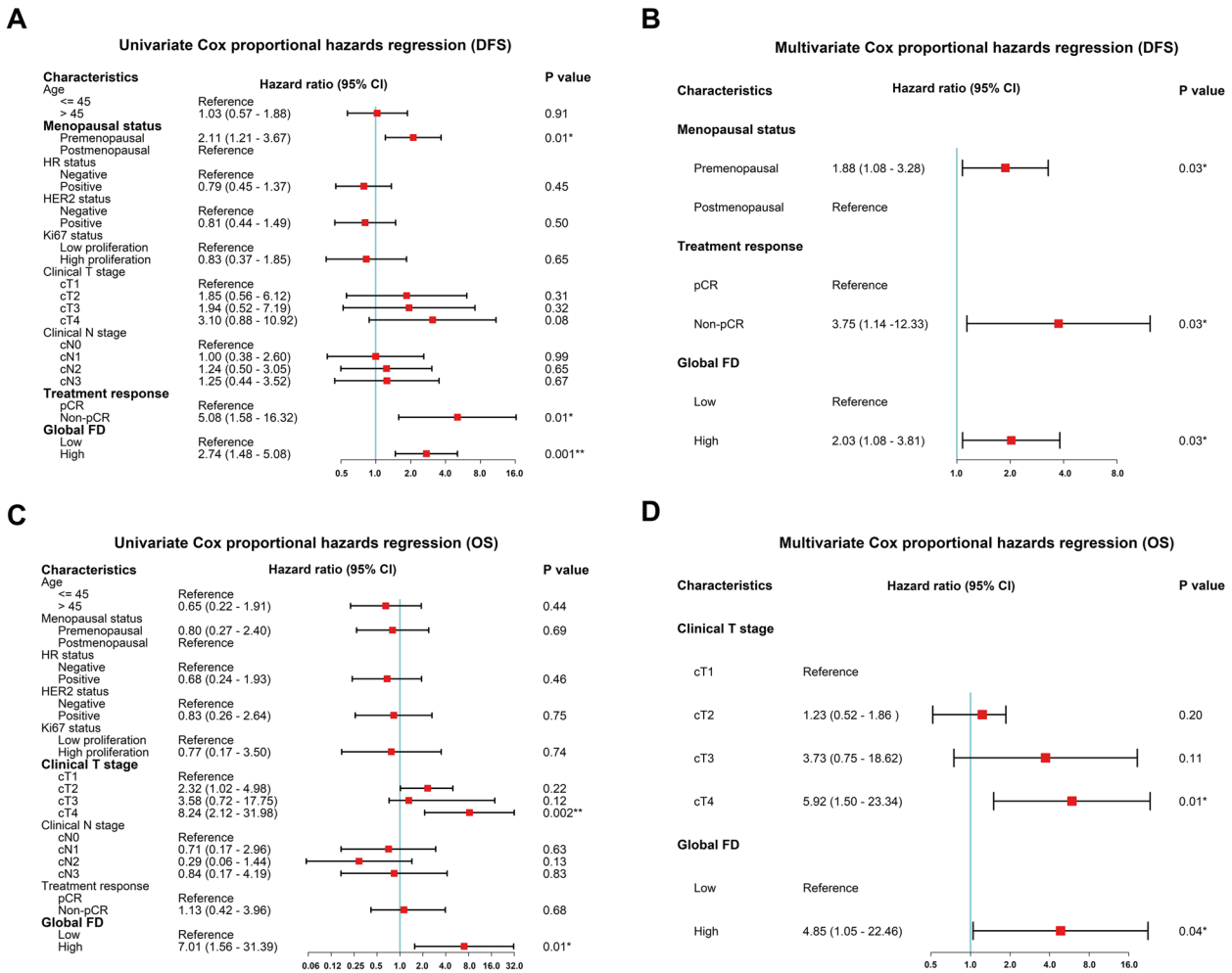

Fig. 5 Forest plots of univariate and multivariate Cox proportional hazards regression analysis of DFS (**A**-**B**) and OS (**C**-**D**). Variables with a *p*-value of less than 0.05 in the univariate Cox proportional hazards regression analysis were included in the multivariate Cox proportional hazards regression analysis. The global FD was identified as an independent prognostic factor for both DFS and OS, with higher global FD values indicating poor prognosis. CI = confidence interval, DFS = disease-free survival, FD = fractal dimension, HER2 = human epidermal growth factor receptor2, HR = hormone receptor, OS = overall survival

Cox proportional hazards analysis identified menopausal status (hazard ratio [HR], 1.88 [95% CI: 1.08, 3.28]; $P = 0.03$), NAC treatment response (HR, 3.75 [95% CI: 1.14, 12.33]; $P = 0.03$) and global FD (HR, 2.03 [95% CI: 1.08, 3.81]; $P = 0.03$) were independent prognostic factors for DFS. While cT4 stage (HR, 5.92 [95% CI: 1.50, 23.34]; $P = 0.01$) and global FD (HR, 4.85 [95% CI: 1.05, 22.46]; $P = 0.04$) were independent prognostic factors for OS (Fig. 5).

For DFS, the cutoff for dividing high and low-risk groups was 11.71, while for OS, the cutoff value was 42.01. Kaplan-Meier analysis for DFS and OS revealed significant differences between the low and high-risk groups (log-rank test, DFS: $P = 0.04$; OS: $P < 0.001$), with the low-risk group exhibiting better DFS and OS (Fig. 6).

Discussion

Accurately predicting pCR to NAC and prognosis in breast cancer patients is crucial for clinical decision-making. This study used fractal analysis to quantify the tumor morphological complexity. The nomogram model combining global FD and clinicopathologic variables (HR status and HER2 status) showed good performance in predicting pCR to NAC. Additionally, the nomogram model that integrated global FD and clinicopathological variables could be used for prognostic stratification in patients with breast cancer.

Previously, tumor morphology descriptions relied mainly on subjective assessments by radiologists and imaging shape features, showing diversity but lacking a quantitative indicator reflecting both tumor size and

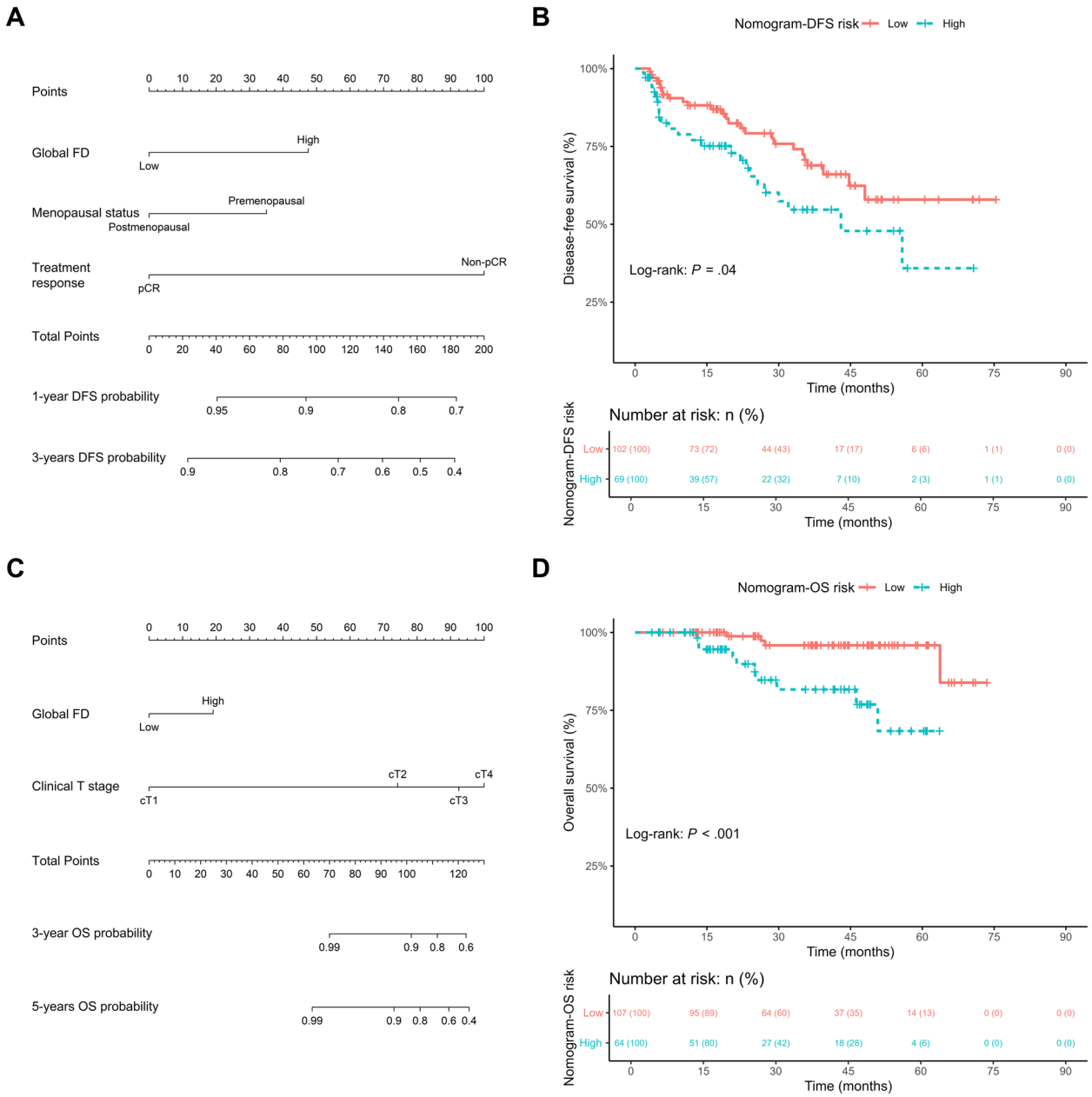

Fig. 6 Prognostic nomogram models and Kaplan-Meier survival curves for DFS (**A**-**B**) and OS (**C**-**D**). Kaplan-Meier analysis showed significant differences in DFS and OS between the low-risk and high-risk groups, with the low-risk group demonstrating better prognosis. DFS = disease-free survival, FD = fractal dimension, OS = overall survival

regularity. FD quantifies tumor morphological complexity without dependence on imaging techniques, which is suitable for broad clinical applications. Previous studies often focused on 2D measurements [16–18]. Variance-components analysis revealed that, compared to global FD, 2D FDs showed a higher coefficient of variation between readings and a lower coefficient of variation between patients. This indicates that global FD may provide a more robust measure and may be beneficial in reflecting patient differences. Spearman correlation analysis revealed that global FD negatively correlates with sphericity, and the surface area to volume ratio, but positively with tumor size; higher morphological complexity (i.e., lower sphericity and larger tumor size) is reflected in increased global FD.

Previous studies have focused on predicting pCR to NAC using clinical TNM staging, HR status, HER2 status, and Ki-67 expression, yet predictions based solely on clinicopathologic variables have shown limitations [38, 39]. Models developed by Li et al [9], based on tumor morphological features, achieved AUCs between 0.69 and 0.81 without further validation. Based on MRI, the radiomics model developed by Liu et al. [32] achieved AUCs ranging from 0.71 to 0.80. Zhuang et al enhanced predictive model performance by combining radiomics and clinicopathologic variables, the combined model achieved an AUC of 0.826 [40]. In this study, the nomogram model-1 (combining global FD, HR status, and HER2 status) achieved AUCs of 0.80 and 0.74, on par with previous studies. Global FD and nomogram model-1 also showed good performance in predicting pCR in subgroup analyses. Notably, global FD offers clinicians an easily understandable quantitative feature, providing interpretability through its depiction of tumor morphology. Our findings suggest the potential of global FD as an imaging biomarker in assisting clinicians to identify pCR before NAC, which was more convenient to calculate than radiomics features.

This study explored the application of global FD in predicting DFS and OS. Our findings indicated that patients with lower nomogram model (combining clinicopathological variables and global FD) scores exhibited better DFS and OS. Cox proportional hazards models indicated global FD was an independent prognostic factor for both DFS and OS. Previous studies have substantiated the importance of MRI tumor morphological features like tumor size in predicting breast cancer prognosis [13, 41, 42]. Our results offer a new perspective on prognostic prediction of breast cancer using non-invasive MRI technology to quantify tumor morphological complexity.

This study has several limitations. First, as a retrospective analysis incorporating data from four centers, the global FD's clinical applicability and effectiveness need further validation through prospective analysis. Second, while this study used semi-automatic segmentation to ensure accuracy in FD calculation, fully automatic techniques could further augment stability and reduce subjectivity. Additionally, the prognostic analysis was based on a limited single-center sample and needs exploration in larger, multi-center cohorts to ascertain the value of global FD in prognosis prediction. Moreover, a comprehensive consideration of tumor morphology and spatial distribution could more fully quantify intratumoral heterogeneity. Finally, given that tumor morphology changes with treatment, reliance on pretreatment images may have limitations. Exploring the value of longitudinal changes in global FD is necessary to predict pCR to NAC and prognosis.

Conclusions

In conclusion, the global FD developed from pretreatment MRI offers a non-invasive and practical approach to quantify the tumor morphological complexity and can predict pCR and prognosis in breast cancer. The generalizability and reproducibility of the prediction model based on the global FD should be validated with larger prospective data sets.

Abbreviations

AUC	Area under the receiver operating characteristic curve
DFS	Disease-free survival
FD	Fractal dimension
HER2	Human epidermal growth factor receptor2
HR	Hormone receptor
NAC	Neoadjuvant chemotherapy
OR	Odds ratio
OS	Overall survival
pCR	Pathologic complete response

Supplementary Information

The online version contains supplementary material available at https://doi.org/10.1186/s13058-025-02034-5.

Supplementary Material 1.

Acknowledgements

The authors thank all the patients who participated in the study, as well as the TCIA database and the I-SPY 2 trial for providing imaging and clinical pathology data.

Authors' contributions

Study design: YH, XXW and JQZ contributed to; Data collection: YC, HFC, XSL, ST; Data analysis: YH, XSL; Accessing and verifying the underlying data: YH, ZTZ, TY; Manuscript editing: YH, XXW, JQZ. All authors reviewed the manuscript, approved the submitted version, and had final responsibility for the decision to submit for publication.

Funding

This study has received funding by the Graduate Research and Innovation Foundation of Chongqing (CYB23070), the Fundamental Research Funds for the Central Universities (2023 CDJYGRH-YB04), Chongqing Medical Research Project of Combination of Science and Medicine (No. 2024MSXM171), the Chongqing University Cancer Hospital Scientific Research Capacity Improvement Project (2023nlts004), and the Natural Science Foundation of Chongqing municipality (CSTB2023NSCQ-MSX0787).

Data availability

No datasets were generated or analysed during the current study.

Declarations

Ethics approval and consent to participate

This study received approval from the ethics committees of all participating institutions. Informed consent was waived due to the retrospective nature of the study.

Competing interests

The authors declare no competing interests.

Author details

[1]School of Medicine, Chongqing University, Chongqing, China. [2]Department of Radiology, Chongqing University Cancer Hospital, Chongqing Key Laboratory for Intelligent Oncology in Breast Cancer (iCQBC), Chongqing 400030, China. [3]Siemens Healthineers Digital Technology (Shanghai) Co., Ltd.,

Shanghai, China. [4]MR Collaborations, Siemens Healthineers Ltd., Chengdu, China.

Received: 19 April 2024 Accepted: 22 April 2025
Published online: 20 May 2025

References

1. Korde LA, Somerfield MR, Carey LA, Crews JR, Denduluri N, Hwang ES, Khan SA, Loibl S, Morris EA, Perez A, et al. Neoadjuvant chemotherapy, endocrine therapy, and targeted therapy for breast cancer: ASCO guideline. J Clin Oncol. 2021;39(13):1485–505.
2. Gradishar WJ, Anderson BO, Abraham J, Aft R, Agnese D, Allison KH, Blair SL, Burstein HJ, Dang C, Elias AD, et al. Breast cancer, version 3.2020, NCCN clinical practice guidelines in oncology. J Natl Compr Canc Netw. 2020;18(4):452–78.
3. Cortazar P, Zhang L, Untch M, Mehta K, Costantino JP, Wolmark N, Bonnefoi H, Cameron D, Gianni L, Valagussa P, et al. Pathological complete response and long-term clinical benefit in breast cancer: the CTNeoBC pooled analysis. Lancet. 2014;384(9938):164–72.
4. Romeo V, Accardo G, Perillo T, Basso L, Garbino N, Nicolai E, Maurea S, Salvatore M. Assessment and prediction of response to neoadjuvant chemotherapy in breast cancer: a comparison of imaging modalities and future perspectives. Cancers (Basel). 2021;13(14):3521.
5. Wolf DM, Yau C, Wulfkuhle J, Brown-Swigart L, Gallagher RI, Lee PRE, Zhu Z, Magbanua MJ, Sayaman R, O'Grady N, et al. Redefining breast cancer subtypes to guide treatment prioritization and maximize response: predictive biomarkers across 10 cancer therapies. Cancer Cell. 2022;40(6):609-623.e606.
6. Caudle AS, Gonzalez-Angulo AM, Hunt KK, Liu P, Pusztai L, Symmans WF, Kuerer HM, Mittendorf EA, Hortobagyi GN, Meric-Bernstam F. Predictors of tumor progression during neoadjuvant chemotherapy in breast cancer. J Clin Oncol. 2010;28(11):1821–8.
7. Braman N, Prasanna P, Whitney J, Singh S, Beig N, Etesami M, Bates DDB, Gallagher K, Bloch BN, Vulchi M, et al. Association of peritumoral radiomics with tumor biology and pathologic response to preoperative targeted therapy for HER2 (ERBB2)-positive breast cancer. JAMA Netw Open. 2019;2(4):e192561.
8. Hylton NM, Blume JD, Bernreuter WK, Pisano ED, Rosen MA, Morris EA, Weatherall PT, Lehman CD, Newstead GM, Polin S, et al. Locally advanced breast cancer: MR imaging for prediction of response to neoadjuvant chemotherapy–results from ACRIN 6657/I-SPY TRIAL. Radiology. 2012;263(3):663–72.
9. Li W, Newitt DC, Gibbs J, Wilmes LJ, Jones EF, Arasu VA, Strand F, Onishi N, Nguyen AA, Kornak J, et al. Predicting breast cancer response to neoadjuvant treatment using multi-feature MRI: results from the I-SPY 2 TRIAL. NPJ Breast Cancer. 2020;6(1):63.
10. Li W, Newitt DC, Yun B, Jones EF, Arasu V, Wilmes LJ, Gibbs J, Nguyen AA, Onishi N, Kornak J, et al. Tumor sphericity predicts response in neoadjuvant chemotherapy for invasive breast cancer. Tomography. 2020;6(2):216–22.
11. Gong X, Wu J, Wu J, Liu J, Gu H, Shen H. Correlation of SASH1 expression and ultrasonographic features in breast cancer. Onco Targets Ther. 2017;10:271–6.
12. Sopik V, Narod SA. The relationship between tumour size, nodal status and distant metastases: on the origins of breast cancer. Breast Cancer Res Treat. 2018;170(3):647–56.
13. Guirguis MS, Adrada BE, Candelaria RP, Sun J, Whitman GJ, Yang WT, Boge M, Mohamed RM, Elshafeey NA, Lane DL, et al. Prediction of response to neoadjuvant systemic therapy in triple negative breast cancer using baseline tumor MRI characteristics and imaging patterns of response. Cancer Res. 2022;82(4):3.
14. Zhang W, Wang Z, Yang S, Wang Y, Xiang S, Guo Z, Hou B, Dong X, Yuan Z, Xu B, et al. Preoperative rim enhancement on magnetic resonance imaging indicates larger tumor size and poor prognosis in Chinese basal-like breast cancer patients. Cancer Biother Radiopharm. 2022;37(8):729–36.
15. Fernández E, Jelinek HF. Use of fractal theory in neuroscience: methods, advantages, and potential problems. Methods. 2001;24(4):309–21.
16. Tochigi T, Kamran SC, Parakh A, Noda Y, Ganeshan B, Blaszkowsky LS, Ryan DP, Allen JN, Berger DL, Wo JY, et al. Response prediction of neoadjuvant chemoradiation therapy in locally advanced rectal cancer using CT-based fractal dimension analysis. Eur Radiol. 2022;32(4):2426–36.
17. Wang J, Li Y, Yang F, Bravo L, Wan K, Xu Y, Cheng W, Sun J, Zhu Y, Zhu T, et al. Fractal analysis: prognostic value of left ventricular trabecular complexity cardiovascular MRI in participants with hypertrophic cardiomyopathy. Radiology. 2021;298(1):71–9.
18. Sherminie LPG, Jayatilake ML. Fractal dimension analysis of pixel dynamic contrast enhanced-magnetic resonance imaging pharmacokinetic parameters for discrimination of benign and malignant breast lesions. JCO Clin Cancer Inform. 2023;7:e2200101.
19. Alvarado-Cruz LB, Delgadillo-Herrera M, Toxqui-Quitl C, Padilla-Vivanco A, Castro-Ortega R, Arreola-Esquivel M. Fractal analysis for classification of breast lesions. In: Conference on current developments in lens design and optical engineering XX: Aug 12 2019. San Diego: Spie-Int Soc Optical Engineering; 2019.
20. Garra BS, Krasner BH, Horii SC, Ascher S, Mun SK, Zeman RK. Improving the distinction between benign and malignant breast lesions: the value of sonographic texture analysis. Ultrason Imaging. 1993;15(4):267–85.
21. Byng JW, Boyd NF, Fishell E, Jong RA, Yaffe MJ. Automated analysis of mammographic densities. Phys Med Biol. 1996;41(5):909–23.
22. Hayward JH, Linden OE, Lewin AA, Weinstein SP, Bachorik AE, Balija TM, Kuzmiak CM, Paulis LV, Salkowski LR, Sanford MF, et al. ACR appropriateness criteria® monitoring response to neoadjuvant systemic therapy for breast cancer: 2022 update. J Am Coll Radiol. 2023;20(5s):S125-s145.
23. Machireddy A, Thibault G, Tudorica A, Afzal A, Mishal M, Kemmer K, Naik A, Troxell M, Goranson E, Oh K, et al. Early prediction of breast cancer therapy response using multiresolution fractal analysis of dce-mri parametric maps. Tomography. 2019;5(1):90–8.
24. Collins GS, Reitsma JB, Altman DG, Moons KG. Transparent reporting of a multivariable prediction model for individual prognosis or diagnosis (TRIPOD): the TRIPOD statement. BMJ. 2015;350:g7594.
25. Brendlin AS, Schmid U, Plajer D, Chaika M, Mader M, Wrazidlo R, Männlin S, Spogis J, Estler A, Esser M, et al. AI denoising improves image quality and radiological workflows in pediatric ultra-low-dose thorax computed tomography scans. Tomography. 2022;8(4):1678–89.
26. Kim M, Kim HS, Kim HJ, Park JE, Park SY, Kim YH, Kim SJ, Lee J, Lebel MR. Thin-slice pituitary MRI with deep learning-based reconstruction: diagnostic performance in a postoperative setting. Radiology. 2021;298(1):114–22.
27. Kwan ML, Bernard PS, Kroenke CH, Factor RE, Habel LA, Weltzien EK, Castillo A, Gunderson EP, Maxfield KS, Stijleman IJ, et al. Breastfeeding, PAM50 tumor subtype, and breast cancer prognosis and survival. J Natl Cancer Inst. 2015;107(7):djv087.
28. Newman LA, Stark A, Chitale D, Pepe M, Longton G, Worsham MJ, Nathanson SD, Miller P, Bensenhaver JM, Proctor E, et al. Association between benign breast disease in African American and White American women and subsequent triple-negative breast cancer. JAMA Oncol. 2017;3(8):1102–6.
29. Tutt A, Tovey H, Cheang MCU, Kernaghan S, Kilburn L, Gazinska P, Owen J, Abraham J, Barrett S, Barrett-Lee P, et al. Carboplatin in BRCA1/2-mutated and triple-negative breast cancer BRCAness subgroups: the TNT trial. Nat Med. 2018;24(5):628–37.
30. Buisseret L, Pommey S, Allard B, Garaud S, Bergeron M, Cousineau I, Ameye L, Bareche Y, Paesmans M, Crown JPA, et al. Clinical significance of CD73 in triple-negative breast cancer: multiplex analysis of a phase III clinical trial. Ann Oncol. 2018;29(4):1056–62.
31. Gómez-Aleza C, Nguyen B, Yoldi G, Ciscar M, Barranco A, Hernández-Jiménez E, Maetens M, Salgado R, Zafeiroglou M, Pellegrini P, et al. Inhibition of RANK signaling in breast cancer induces an anti-tumor immune response orchestrated by CD8+ T cells. Nat Commun. 2020;11(1):6335.
32. Liu Z, Li Z, Qu J, Zhang R, Zhou X, Li L, Sun K, Tang Z, Jiang H, Li H, et al. Radiomics of multiparametric MRI for pretreatment prediction of pathologic complete response to neoadjuvant chemotherapy in breast cancer: a multicenter study. Clin Cancer Res. 2019;25(12):3538–47.
33. Leithner D, Horvat JV, Marino MA, Bernard-Davila B, Jochelson MS, Ochoa-Albiztegui RE, Martinez DF, Morris EA, Thakur S, Pinker K. Radiomic signatures with contrast-enhanced magnetic resonance imaging for the assessment of breast cancer receptor status and molecular subtypes: initial results. Breast Cancer Res. 2019;21(1):106.

34. Kempkes SN, Slot MR, Freeney SE, Zevenhuizen SJM, Vanmaekelbergh D, Swart I, Smith CM. Design and characterization of electrons in a fractal geometry. Nat Phys. 2019;15(2):127–31.
35. Liu S, Fan X, Zhang C, Wang Z, Li S, Wang Y, Qiu X, Jiang T. MR imaging based fractal analysis for differentiating primary CNS lymphoma and glioblastoma. Eur Radiol. 2019;29(3):1348–54.
36. van Griethuysen JJM, Fedorov A, Parmar C, Hosny A, Aucoin N, Narayan V, Beets-Tan RGH, Fillion-Robin JC, Pieper S, Aerts H. Computational radiomics system to decode the radiographic phenotype. Cancer Res. 2017;77(21):e104–7.
37. Sanghera B, Banerjee D, Khan A, Simcock I, Stirling JJ, Glynne-Jones R, Goh V. Reproducibility of 2D and 3D fractal analysis techniques for the assessment of spatial heterogeneity of regional blood flow in rectal cancer. Radiology. 2012;263(3):865–73.
38. Arici S, Sengiz Erhan S, Geredeli C, Cekin R, Sakin A, Cihan S. The clinical importance of androgen receptor status in response to neoadjuvant chemotherapy in Turkish patients with local and locally advanced breast cancer. Oncol Res Treat. 2020;43(9):435–40.
39. Ouldamer L, Bendifallah S, Pilloy J, Arbion F, Body G, Brisson C, Lavoué V, Lévêque J, Daraï E. Risk scoring system for predicting breast conservation after neoadjuvant chemotherapy. Breast J. 2019;25(4):696–701.
40. Zhuang X, Chen C, Liu Z, Zhang L, Zhou X, Cheng M, Ji F, Zhu T, Lei C, Zhang J, et al. Multiparametric MRI-based radiomics analysis for the prediction of breast tumor regression patterns after neoadjuvant chemotherapy. Transl Oncol. 2020;13(11):100831.
41. Kim JY, Kim JJ, Hwangbo L, Suh HB, Kim S, Choo KS, Nam KJ, Kang T. Kinetic heterogeneity of breast cancer determined using computer-aided diagnosis of preoperative MRI scans: relationship to distant metastasis-free survival. Radiology. 2020;295(3):517–26.
42. Liang T, Hu B, Du H, Zhang Y. Predictive value of T2-weighted magnetic resonance imaging for the prognosis of patients with mass-type breast cancer with peritumoral edema. Oncol Lett. 2020;20(6):314.

Publisher's Note

Springer Nature remains neutral with regard to jurisdictional claims in published maps and institutional affiliations.